Acta Oceanol. Sin., 2024, Vol. 43, No. 2, P. 11–22
https://doi.org/10.1007/s13131-023-2223-5
http://www.aosocean.com
E-mail: ocean2@hyxb.org.cn

Effect of particle composition and consolidation degree on the wave-induced liquefaction of soil beds

Zhiyuan Chen[1,2,3], Yupeng Ren[4], Guohui Xu[1,3]*, Meng Li[1,3]

[1] Shandong Provincial Key Laboratory of Marine Environment and Geological Engineering, Ocean University of China, Qingdao 266100, China

[2] Marine Ecological Restoration and Smart Ocean Engineering Research Center of Hebei Province, Qinhuangdao 066000, China

[3] Key Laboratory of Marine Environment and Ecology (Ocean University of China), Ministry of Education, Qingdao 266100, China

[4] Key Laboratory of Submarine Geoscience and Prospecting Techniques (Ocean University of China), Ministry of Education, Qingdao 266100, China

Received 6 January 2023; accepted 23 June 2023

Abstract

The wave-induced liquefaction of seabed is responsible for causing damage to marine structures. Particle composition and consolidation degree are the key factors affecting the pore water pressure response and liquefaction behavior of the seabed under wave action. The present study conducted wave flume experiments on silt and silty fine sand beds with varying particle compositions. Furthermore, a comprehensive analysis of the differences and underlying reasons for liquefaction behavior in two different types of soil was conducted from both macroscopic and microscopic perspectives. The experimental results indicate that the silt bed necessitates a lower wave load intensity to attain the liquefaction state in comparison to the silty fine sand bed. Additionally, the duration and development depth of liquefaction are greater in the silt bed. The dissimilarity in liquefaction behavior between the two types of soil can be attributed to the variation in their permeability and plastic deformation capacity. The permeability coefficient and compression modulus of silt are lower than those of silty fine sand. Consequently, silt is more prone to the accumulation of pore pressure and subsequent liquefaction under external loading. Prior research has demonstrated that silt beds with varying consolidation degrees exhibit distinct initial failure modes. Specifically, a dense bed undergoes shear failure, whereas a loose bed experiences initial liquefaction failure. This study utilized discrete element simulation to examine the microscopic mechanisms that underlie this phenomenon.

Key words: wave flume, liquefaction, pore water pressure, consolidation permeability experiment, discrete element simulation

Citation: Chen Zhiyuan, Ren Yupeng, Xu Guohui, Li Meng. 2024. Effect of particle composition and consolidation degree on the wave-induced liquefaction of soil beds. Acta Oceanologica Sinica, 43(2): 11–22, doi: 10.1007/s13131-023-2223-5

1 Introduction

The wave-induced liquefaction of the seabed is a common submarine geological disaster. Liquefied soil is fluid and loses its bearing capacity, causing harm to marine structures (de Groot et al., 2006; Kirca, 2013; Kirca and Sumer, 2018; Sumer et al., 1999, 2006a, 2006c, 2011; Xu et al., 2019). The soil properties and external wave load intensity are key factors determining whether liquefaction will occur in the seabed. (Duan et al., 2017; Guo et al., 2014; Liu et al., 2009; Zhao et al., 2016). Particle composition and consolidation degree are important indicators to measure soil properties. They have an important impact on the response characteristics of pore water pressure and liquefaction of the seabed under wave loads (Gao et al., 2011; Ren et al., 2020a; Wang et al., 2016; Zhao et al., 2018). However, there are few studies on the macroscopic and microscopic causes of their effects on seabed liquefaction, which is of great significance to further reveal the mechanism of seabed liquefaction.

In the past few decades, researchers have conducted extensive studies on wave-induced liquefaction of the seabed. Through field investigations, the possibility for wave-induced liquefaction of silt and silty fine sand has been demonstrated, either directly through monitoring of pore water pressure during storm events or indirectly through geological and geomorphic analyses of the seabed (Prior et al., 1989; Sassa et al., 2006; Xu et al., 2009; Xu et al., 2021; Zen and Yamazaki, 1991). Theoretical models have been proposed to predict the response of pore water pressure in the seabed subjected to wave load. These models take into account the elasticity and elastoplasticity of the seabed soil (Biot, 1956; Jeng and Rahman, 2000; Jeng and Cha, 2003; Sassa and Sekiguchi, 2001; Sassa et al., 2001; Yamamoto et al., 1978; Zienkiewicz et al., 1980). In order to address the issue of fluid-structure-seabed interaction, Ye et al. (2013) developed a two-dimensional semi-coupled model, FSSI-CAS 2D, and applied it to the calculation of pore water pressure response in seabed soil under

Foundation item: The National Natural Science Foundation of China under contract No. 41976049; the Opening Foundation of Marine Ecological Restoration and Smart Ocean Engineering Research Center of Hebei Province under contract No. HBMESO2306.
*Corresponding author, E-mail: xuguohui@ouc.edu.cn

different dynamic loads and buried structures (Yang and Ye, 2017, 2018; Ye and He, 2021). Based on these theoretical models and liquefaction criteria, the wave-induced liquefaction depth of the seabed can be determined (Jeng, 1997; Okusa, 1985; Tsai, 1995; Ye, 2012; Ye and Wang, 2015; Zen and Yamazaki, 1990a). The response characteristics of pore water pressure in seabed can be revealed through various experimental methods such as wave flume experiments, centrifuge experiments, and one-dimensional cylindrical pressure experiments. The pore water pressure can be classified into two types based on the characteristics of its fluctuation and accumulation, namely instantaneous and accumulative pore water pressure (Foda and Tzang, 1994; Liu et al., 2015; Zen and Yamazaki, 1990a, 1990b). Numerous experimental results indicate that wave-induced liquefaction of the seabed is characterized by a progressive development from top to bottom (Kirca et al., 2013; Sassa and Sekiguchi, 1999; Sumer et al., 2006b). Soil in a liquefied state will move elliptically, which is similar to the overlying water column under wave action (Cao et al., 2019; Chen et al., 2019; Miyamoto et al., 2020; Ren et al., 2020b; Xu et al., 2012), and the liquefied soil particles will deposit due to the fluctuation sorting after reaching the maximum liquefaction depth (Miyamoto et al., 2004; Ren et al., 2021; Xu et al., 2016). These experimental results are reflected in the liquefaction research of both silt and sand.

The liquefaction laws of silt and sand exhibit several similarities, but their respective permeability and mechanical properties differ significantly due to the difference in particle composition. Consequently, the pore water pressure response characteristics and liquefaction behavior of two types of soil under wave action are expected to differ markedly. The performance and reasons for this difference are noteworthy. According to previous studies, permeability and plastic deformation are the key factors causing pore pressure accumulation and liquefaction (Duan et al., 2019; Madsen, 1978; Wu and Jeng, 2019; Ye et al., 2018). At the same time, the physical and mechanical properties of soil are macroscopic reflections of its internal micro particle arrangement and structure characteristics. Tzang and Ou (2006) studied the pore pressure response of two kinds of fine sand with different median particle diameters and found that the coarser sand exhibited a non-fluidization response, while the finer sand demonstrated fluidization. Kirca et al., 2014 and Zhang et al., 2020 found that the clay content of the seabed has an important influence on the development of pore water pressure through flume experiments. Using scanning electron microscopy (SEM), Gratchev et al. (2006) found that soil that is prone to liquefaction has an open microfabric. Therefore, it is necessary to study the influence of micro particle characteristics in soil on the pore water pressure response of the seabed. In addition, Ren et al. (2020a) found that silt beds with different consolidation degrees have different initial failure modes. Therefore, it can be inferred that as the degree of consolidation increases, the internal particle arrangement characteristics of the soil will inevitably change.

This paper had conducted wave flume experiment on silty fine sand to investigate its dynamic response under wave action. The particle diameters composition of the silty fine sand was similar to that of silt. The experimental results were compared with those of previous silt bed experiment (Ren et al., 2020a) to investigate the influence of particle composition on pore water pressure response and liquefaction behavior of soil beds. Furthermore, the microscale reasons for the distinct initial failure modes exhibited by soil beds with varying consolidation degrees were investigated through the discrete element simulation.

2 Methods

2.1 *Flume experiment*

Based on the observed phenomena and results from previous experiments (Sassa and Sekiguchi, 1999; Sumer et al., 2006b), the wave load intensity necessary to induce soil bed liquefaction, the maximum development depth of liquefaction, and the duration of liquefaction were considered as metrics to assess the liquefaction potential and behavior of soil beds.

2.1.1 *Instruments and equipment*

The main equipment for the wave flume experiment was a push-plate wave flume with dimensions of 14 m in length, 0.5 m in width and 1.5 m in height. A soil container was set up in the middle of the flume, measuring 2.6 m in length, 0.5 m in width and 0.6 m in height. The left end of the flume was equipped with a 1:4 slope wave elimination section, while the right end was equipped with a push plate to generate traveling waves (Fig. 1).

Prior to soil beds laying, pore water pressure sensors were fixed onto a steel wire (model: the CYY2 sensor produced by Xi'an Micropositive Electronic Technology Co., Ltd; accuracy: 0.5%). The steel wire was vertically aligned and secured at the center of the soil container. In order to eliminate air bubbles within the pore water pressure sensors and ensure that the sensors were in a saturated state, the sensors were immersed in cold boiled water for 24 hours prior to deployment. The pore water pressure sensors were installed at three depths within soil beds, with the locations of the silt bed sensors located at depths of 0.21 m, 0.37 m, and 0.45 m below the bed surface, while the locations of the silty

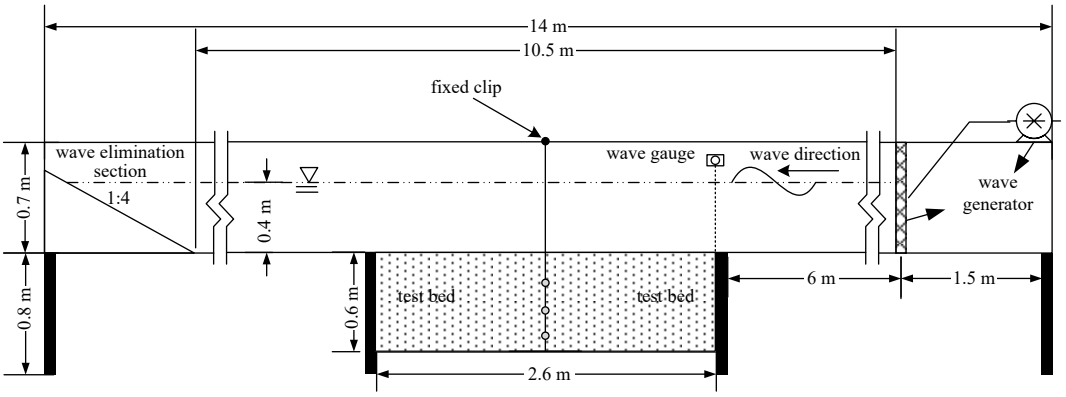

Fig. 1. Schematic diagram of the wave flume device.

fine sand bed sensors were positioned at depths of 0.25 m, 0.35 m, and 0.45 m below the bed surface. The specific layout of the sensors is presented in Fig. 2.

2.1.2 *Soil properties and laying method*

The silty fine sand used in this experiment was taken from Caofeidian, Hebei Province, and the median particle diameter d_{50} is 0.138 mm. Silt was taken from the Huanghe River Delta, with a median particle diameter d_{50} of 0.046 mm and a clay content of 11.42%. The grain diameter grading curves of the two soils are shown in Fig. 3.

The sifted silt and silty fine sand were mixed with water, configured as test soils with a moisture content of 32% and 28%, respectively, and laid in the soil container of the wave flume. To ensure the uniformity of soil beds as much as possible, soil beds were laid using the sliding along flat method, the laying size of soil beds were 2.6 m × 0.5 m × 0.6 m (Fig. 1). After the completion of the soil beds laying, water was injected to a height of 40 cm. Subsequently, soil beds were allowed to self-weight consolidation for 7 days. Prior to conducting the experiment, soil bed sampling was performed and the soil moisture content was determined using the drying method. The WG-V foundation bearing capacity tester was then utilized to measure the penetration resistance of the test soil beds (Fig. 4). From Fig. 4, it can be observed that both the silt and silty fine sand beds undergone a certain degree of decrease in their moisture content after 7 days of self-weight consolidation. Regarding the penetration resistance, the internal penetration resistance of the silt bed was significantly greater than that of the silty fine sand bed. Even after prolonged consolidation, the strength of the sand bed remained relatively low. This may indicate that a certain soil structure is formed within the silt bed during consolidation, thus providing it with higher strength, whereas the silty fine sand bed lacks this characteristic.

2.1.3 *Test conditions and process*

During the wave flume experiment, the wave conditions applied to the silty fine sand bed were identical to those of the previous the silt bed experiment (Ren et al., 2020a). The experiment commenced by subjecting the soil bed to waves with wave heights of 6 cm and 10 cm for a duration of 120 minutes. Subsequently, the wave heights were increased to 18 cm until the completion of the experiment (Table 1). The measurement of wave parameters was performed using the WG-55 wave gauge produced by RBR Canada, with an accuracy of 0.15%.

Throughout the experiment, real-time values of wave parameters and pore water pressures within soil beds were collected by DEWESoft data acquisition instrument (model: DEWE-43; acquisition frequency: 50 Hz). The occurrence and depth of soil bed liquefaction were determined through the fluctuation in soil beds observed through the transparent sidewall of the wave flume.

2.2 *Consolidation permeability experiment*

In order to analyze the reasons for the differential dynamic responses of silt and silty fine sand beds under wave action, consolidation and permeability experiments were conducted on the two types of soil. The silt and silty fine sand in the experiment were identical to those used in the flume experiment. The consolidation experiment was conducted using a customized GJ-16 consolidation apparatus. The soil specimen was a cylinder measuring 6.1 cm in diameter and 4 cm in height, this dimension ensures

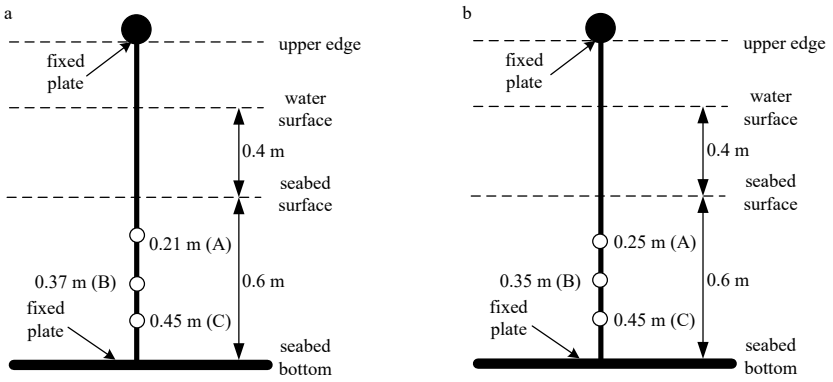

Fig. 2. Layout diagram of pore water pressure sensors (a. silt bed; b. silty fine sand bed).

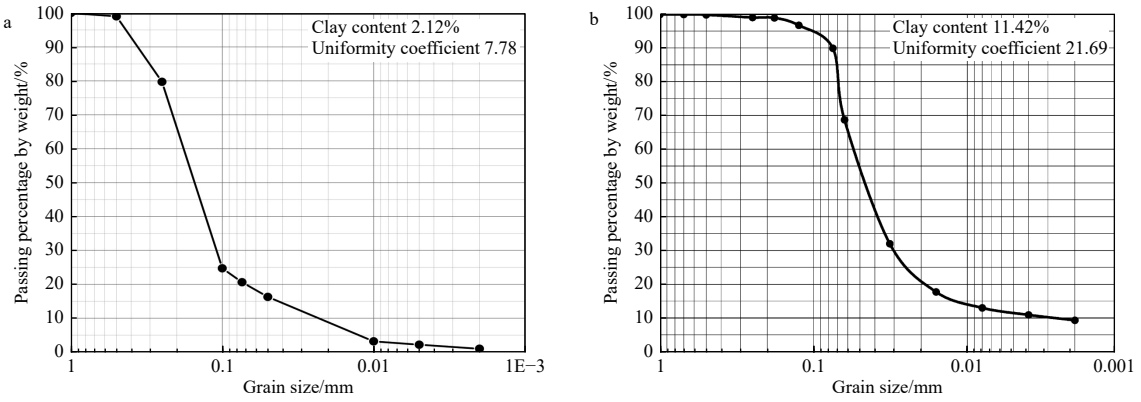

Fig. 3. Grain diameter grading curve of the test soil (a. silty fine sand; b. silt).

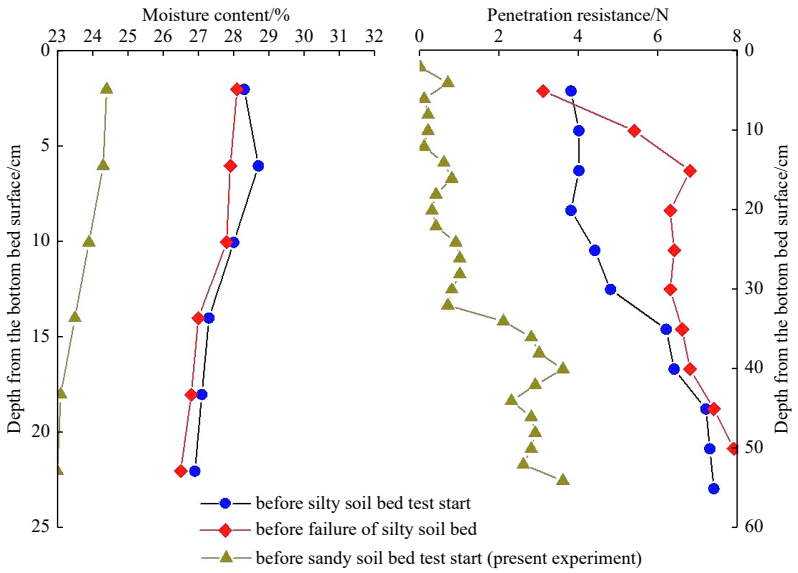

Fig. 4. Comparison of the moisture content and penetration resistance for silt and silty fine sand bed.

Table 1. The order of waves applied in the experiment

Flume experiment of the silty fine sand bed
Applying wave height H = 6 cm for 120 min
Applying wave height H = 10 cm for 120 min
Applying wave height H = 18 cm to the end of the experiment (90 min)

that the compressed soil specimen can be transferred to the permeameter for testing. During the consolidation process, the consolidation method was the undrained consolidation, and a total of 7 consolidation pressures were applied, namely, 0 kPa, 12.5 kPa, 25 kPa, 50 kPa, 100 kPa, 150 kPa and 200 kPa. Among them, the silt specimens were compressed for 8 hours, while the silty fine sand specimens were 4 hours (based on the pretest results, the compression displacement of silt and silty fine sand remained unaltered when subjected to pressure for 8 hours and 4 hours, respectively). Following the consolidation experiment, the compression displacement of the specimen was recorded, and subsequently transferred to a permeameter for permeability testing with minimal disturbance. In order to eliminate the influence of height reduction of soil specimen after compression on the results of permeability experiment, a layer of coarse sand was placed on the surface of the soil specimen to maintain its original height (prior to consolidation). The permeability experiment was conducted by employing a variable head permeameter for measuring the permeability of silt and a constant head permeameter for measuring the permeability of silty fine sand, taking into consideration the difference in permeability of the two types of soil. For ensuring the representativeness of the experimental outcomes, three sets of parallel experiments were executed for each consolidation pressure condition throughout the consolidation permeability experiment, with the average values of the three sets of results being measured to diminish the impact of errors on the experimental data.

2.3 *Discrete element simulation*

The physical and mechanical properties of soil are the macroscopic reflection of its internal microstructure characteristics. In this study, the discrete element method was utilized to simulate the changes in particle arrangement and pore space inside silt and silty fine sand during consolidation experiments, and the differences in micro particle arrangement between the two types of soil were investigated.

The software utilized was Particle Flow Code (PFC). Considering the tradeoff between sample representativeness and computational efficiency, the quantity of particles generated for silt and silty fine sand ranged between 20 000 and 30 000 in accordance with the grain diameter grading curve of the soil utilized in the flume experiment. The sample size generated by discrete element simulation was scaled down proportionally with respect to the size of the sample for consolidation permeability experiment. The generated silt sample measured 2 mm × 3 mm, while the silty fine sand sample measured 20 mm × 30 mm, resulting in 21 769 particles for silt and 22 063 particles for silty fine sand (Fig. 5). The linear model was employed for inter-particle contact, where the normal stiffness k_n was 2×10^8 N/m, the tangential stiffness k_s was 2×10^8 N/m, and the coefficient of friction between particles was 0.3.

To compress the generated samples, a displacement-controlled loading method was implemented. The model's upper boundary was set as an active boundary, while the remaining boundaries were fixed. The compression displacements of two soil samples at each loading in the consolidation experiment were converted to the corresponding compression displacements in the discrete element simulation based on the size ratios. Subsequently, the samples were subjected to compression and the changes in the microscopic particle arrangement were recorded after each loading was applied.

3 Results and discussions

3.1 *Soil bed liquefaction behavior: silt vs. silty fine sand*

The pore water pressure response curves of silt and silty fine sand bed are presented in Figs 6 and 7, and the residual pore water pressure can be obtained using the following equation:

$$\bar{p} = \frac{\int_t^{t+T} p\mathrm{d}t}{T}.$$

where $\bar{p}$ is the residual pore water pressure, p is the real-time pore water pressure， t is time, and T is the wave period.

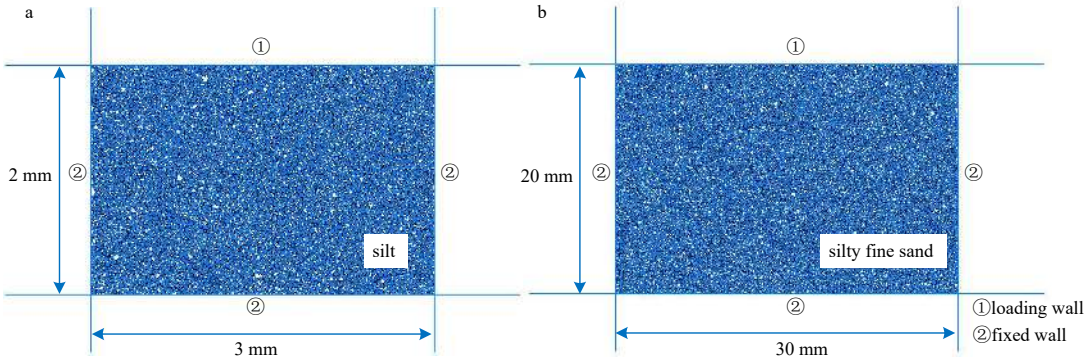

Fig. 5. Discrete element model setup (a. silt; b. silty fine sand).

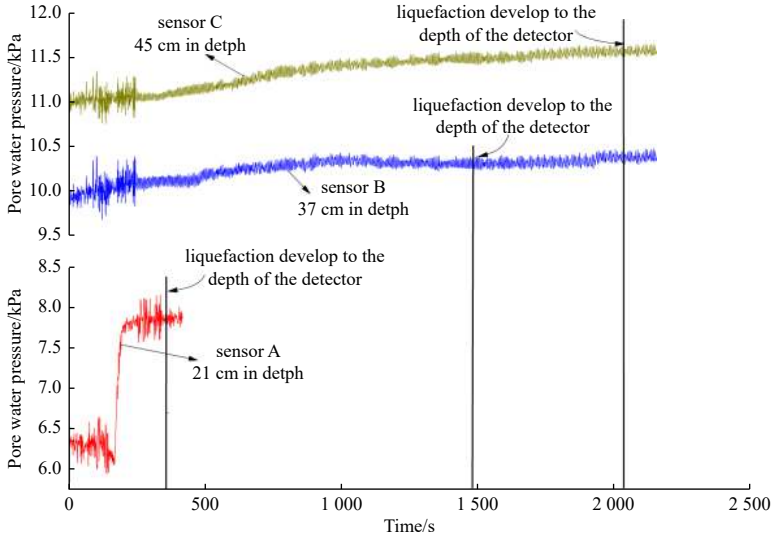

Fig. 6. Response of the pore pressure in the silt bed when H = 18 cm (modified from Ren et al. (2020a)).

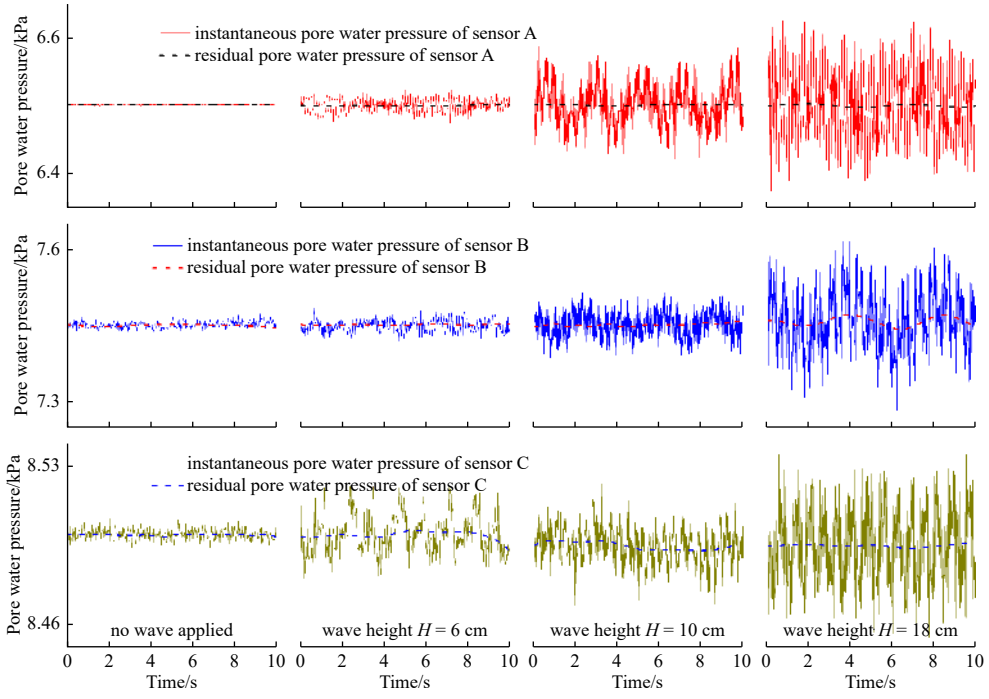

Fig. 7. Response of the pore pressure in the silty fine sand bed under wave action.

For the silt bed, the pore water pressure at different depths remained stable when the wave height was 6 cm and 10 cm (Ren et al., 2020a). However, when the wave height increased to 18 cm, there was a sharp accumulation of pore water pressure at a depth of 21 cm in the silt bed, leading to liquefaction. The pore water pressure at other depths also gradually accumulated and eventually led to liquefaction (Fig. 6).

For the silty fine sand bed, the pore water pressure exhibited periodic oscillations around the hydrostatic pressure at different depths, and the amplitude of the oscillations was found to increase with an increase in wave height. However, it is observed that even with a significant increase in wave height up to 18 cm, pore water pressure did not accumulate within the sand bed (Fig. 7). The silty fine sand bed remained stable and no fluctuation of the bed could be observed through the glass sidewall (Table 2).

After the wave height increased to 18 cm, the accumulation of pore water pressure occurred in the silt bed at different depths. The accumulation rate was the fastest at a depth of 21cm, while the pore pressure accumulation in deeper layers was relatively slow. In contrast, the silty fine sand bed only exhibited elastic response to wave loads even under the dynamic conditions of a wave height of 18 cm, and there was no occurrence of pore pressure accumulation. Due to the limitations of wave flume dimensions, the wave-induced hydrodynamic loads could not be further increased. In order to induce liquefaction of the silty fine sand bed, artificial disturbance was applied to the bed. The disturbance was performed by using a rectangle hammer with dimensions of 10 cm × 15 cm and a weight of 3.5 kg to repeatedly strike the bed surface (hammering the bed surface downward during wave crests and lifting the hammer during wave troughs), with the frequency of artificial disturbance equal to the wave frequency. The disturbance stopped immediately after the fluctuation of the bed and the variation in pore water pressure were observed. The pore water pressure response in the silty fine sand bed after an artificial disturbance is shown in Fig. 8.

Following an artificial disturbance, the pore water pressure in the silty fine sand bed rapidly accumulated. However, this accumulation was confined to the location of sensors A and B, while the position of sensor C remained unaffected by the disturbance. Additionally, the extent of the pore water pressure rise was considerably smaller than that observed in the silt bed. Specifically, the range of the pore water pressure rise at sensors A and B was limited to 0.6 kPa. Based on the observation of soil bed fluctuation through the glass sidewall of the flume, the silty fine sand bed was liquefied only within a shallow surface layer of 6.6 cm. In comparison to the silt bed, the silty fine sand bed had a significantly reduced liquefaction depth. Moreover, the whole liquefaction process in the silty fine sand bed was brief, and the excess pore water pressure caused by artificial disturbance dissipated completely within 143 s only.

It is noteworthy that the pore water pressure values in Figs. 6, 7, and 8 exhibited different characteristics over time. The pore water pressure values in Figs 6 and 8 accumulated under external loading, indicating the occurrence of soil beds liquefaction failure. After liquefaction, the pore pressure within the silt bed reached a peak value and could remain stable for a long time (Fig. 6). In contrast, the pore pressure within the silty fine sand bed dissipated quickly (Fig. 8), implying that the duration of liquefaction is longer for silt bed than for silty fine sand bed. Fig. 7 displayed a steady change in pore pressure over time, mainly because the fine sand bed remained stable under 18 cm wave height wave action. Therefore, based on the experimental phenomena and data described above, the liquefaction behaviors of two soil beds are summarized in Table 3.

It can be seen that the silt bed is more prone to liquefaction compared to the silty fine sand bed. This can be attributed to the following manifestations: (1) the silt bed requires less dynamic load from waves to reach the state of liquefaction as compared to the silty fine sand bed; and (2) after reaching the state of liquefaction, the silt bed undergoes a greater development depth and duration of liquefaction compared to the silty fine sand bed.

3.2 *Analysis of the reasons for differences in soil bed liquefaction behavior*

3.2.1 *Macroscopic physical properties differences in silt and silty fine sand*

de Groot et al. (2006) summarized the cases of damage to a seabed under various field conditions and proposed the concept of a characteristic drainage period. It is considered that the accumulation of pore water pressure will occur only when the time required to produce a specific excess pore water pressure is less than the time required to dissipate the pressure due to drainage. The accumulation and dissipation of pore water pressure are closely related to the plastic deformation and permeability of soil. Existing studies have only indicated that the permeability of fine sand is greater than that of silt, and with the increase of consolidation degree, the permeability of both will decrease. However, there has been no specific study on the permeability and deformation variation degrees of two types of soil with increasing consolidation pressure. In this study, a combined method of consolidation and permeability experiments was used to explore the changes in the plastic deformation ability and permeability of silt and silty fine sand under external forces.

During the experiment, the applied consolidation pressures were 0 kPa, 12.5 kPa, 25 kPa, 50 kPa, 100 kPa, and 200 kPa. The compression displacements of the silt and silty fine sand under each consolidation pressure condition are presented in Table 4.

A comparison curve of the compression displacements of two types of soil under various levels of consolidation pressure is shown in Fig. 9.

According to Table 4 and Fig. 9, it can be observed that as the consolidation pressure increased, the heights of the silt and silty fine sand specimens steadily decreased. However, when the consolidation pressure increased from 12.5 kPa to 200 kPa, the compression displacement of the silt specimen increased by 1.698 mm, while that of the silty fine sand specimen only increased by 0.669 mm. The compression modulus $E_{S\,(1\text{-}2)}$ calculated when the consolidation pressure increased from 100 kPa to 200 kPa was se-

Table 2. Changes in pore water pressure of silt and silty fine sand bed during experiments

Silt bed	Silty fine sand bed
When H = 6 cm, the pore water pressure of the soil remained stable.	When H = 6 cm, the pore water pressure of the soil remained stable.
When H = 10 cm, the pore water pressure of the soil still remained stable.	When H = 10 cm, the pore water pressure of the soil remained stable.
When H = 18 cm, the pore water pressure began to increase in all layers of the seabed.	When H = 18 cm, the pore water pressure of the soil still remained stable.

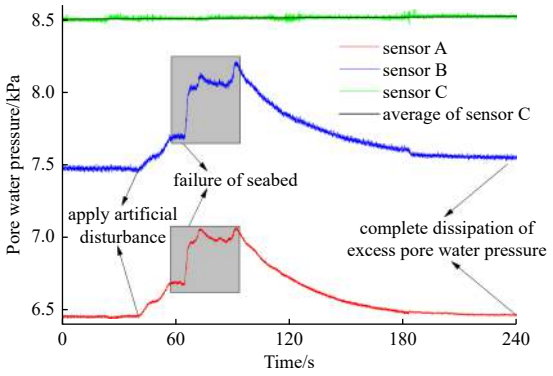

Fig. 8. Response of the pore pressure in the silty fine sand bed after the artificial disturbance.

lected as the index to represent the plastic deformation capacity of soil. After the calculation, the compression modulus $E_{S\,(1\text{-}2)}$ of silt and silty fine sand were 5.67 MPa and 19.90 MPa, respectively, and the latter was 3.5 times greater than the former. Therefore, the silt bed is more prone to plastic deformation than the silty fine sand bed under external load. The permeability experiment was carried out on the soil samples compressed under various levels of consolidation pressure, and the variation relationship between the permeability coefficient of the soil sample and the consolidation pressure is displayed in Fig. 10.

Notably, the permeability coefficient of silt was significantly lower in comparison to silty fine sand. A gradual decrease in permeability coefficient was observed as the consolidation pressure increased in both soils. Throughout this process, the silt sample exhibited a reduction in permeability coefficient of 67.4% as compared to its initial state at a consolidation pressure of 0 kPa, whereas the sand sample demonstrated a reduction of only 28.6%.

3.2.2 *Microscopic arrangement characteristics of particles in silt and silty fine sand*

The permeability coefficient of the silt is significantly smaller than that of the silty fine sand. The physical and mechanical properties of the soil are a macroscopic reflection of its internal microscopic characteristics. In order to investigate the reasons for the significant difference in permeability between the two soils, the discrete element simulation has been utilized to investigate the microscopic particle arrangement characteristics of silt and silty fine sand. The generated samples from Fig. 5 were zoomed in on a specific region to explore the differences in micro arrangement characteristics of particles in silt and silty fine sand. The specific simulation results are shown in Fig. 11.

According to the simulation results, obvious differences in the arrangement of microparticles between the silt and silty fine sand were observed, which is an important reason for the great difference in permeability between the two soils, which is embodied in the following aspects:

(1) First, there exists a considerable variation in the diameter of particles within silt, as evidenced by a nonuniformity coefficient of 21.69. The interstitial gaps situated between larger silt and sand particles are vulnerable to filling via the intrusion of smaller clay particles, thereby resulting in a marked decrease in overall porosity, as well as a constriction of water seepage pathways. Simultaneously, several studies have demonstrated the existence of a hydration film on the clay particle surface, which originates from electrostatic adsorption. The thickness range of hydration film is typically acknowledged to vary in the 0-200 nm

Table 3. Comparison of the liquefaction behavior of the silt and silty fine sand beds

Soil type	Wave height required for liquefaction/cm	Maximum liquefaction depth/cm	Liquefaction duration
Silt	18	45.0	>250 min
Silty fine sand	>18	6.6	2 min 23 s

Note: The silt bed data come from Ren et al. (2020a) test 1, and the maximum liquefaction depth and duration of liquefaction were obtained under wave load with wave height H = 18 cm.

Table 4. Compression displacement of silt and silty fine sand under different consolidation pressures

Consolidation pressure	12.5 kPa	25 kPa	50 kPa	100 kPa	150 kPa	200 kPa
Silt/mm	2.442	2.998	3.329	3.435	4.011	4.140
Silty fine sand/mm	0.086	0.189	0.310	0.554	0.630	0.755

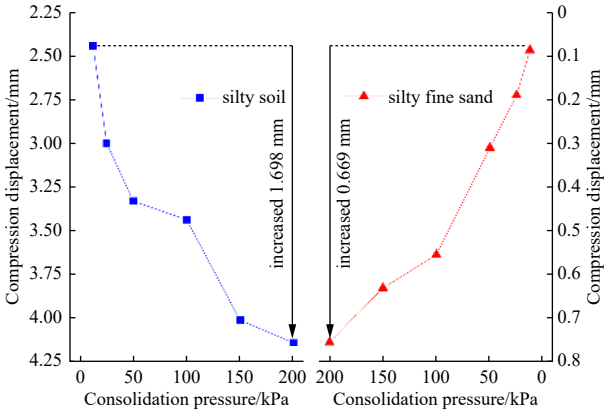

Fig. 9. Change in the compression displacement of the two kinds of soil with increasing consolidation pressure.

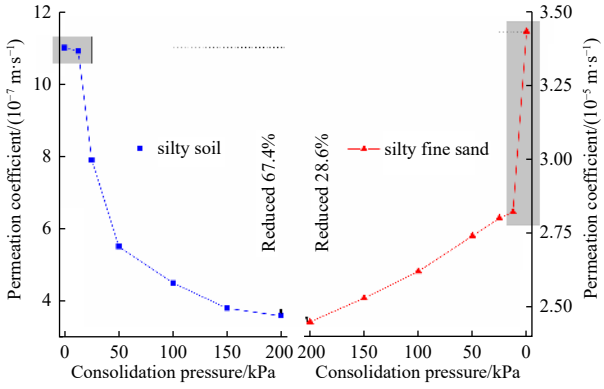

Fig. 10. Change in the permeability coefficient of the two kinds of soil with increasing consolidation pressure.

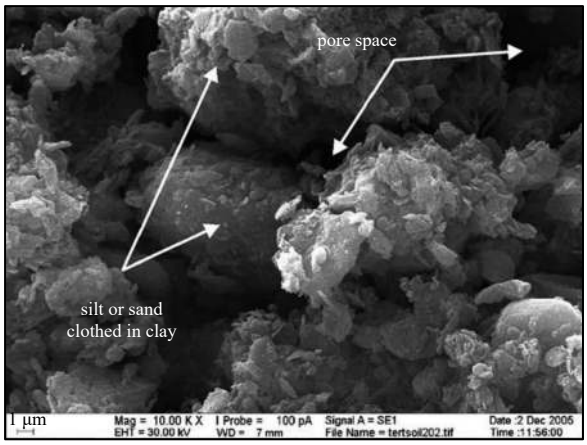

a. SEM image of Terano landslide soil with a clay content of 11% (quoted from Gratchev et al. (2006))

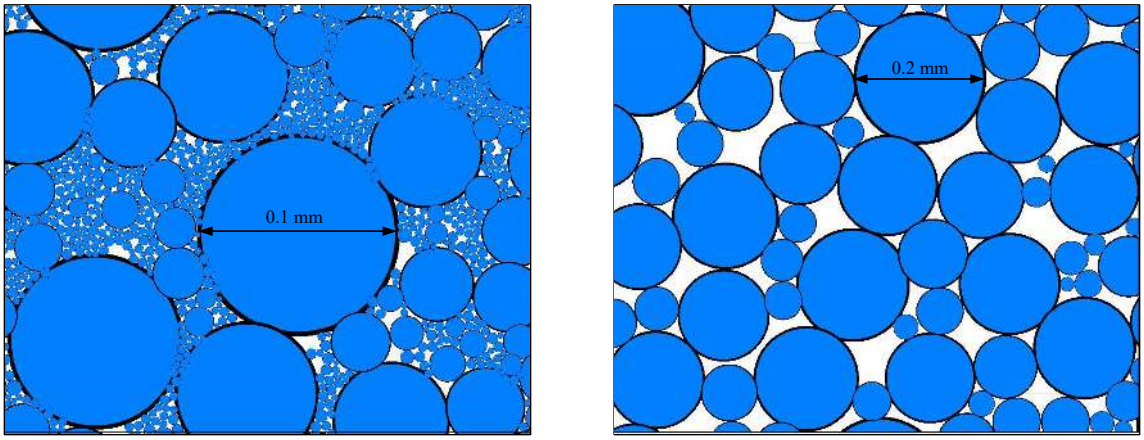

b. Sample image of silt

c. Sample image of silty fine sand

Fig. 11. Discrete element sample images of silt and silty fine sand.

range (Peng et al., 2015). Furthermore, the existence of the hydration film is believed to decrease the seepage space and cause a decrease in the silt's permeability. Nevertheless, the particles diameter of silty fine sand exhibits a high degree of uniformity as evidenced by its nonuniformity coefficient of 7.78. The pore space between particles of silty fine sand is relatively large. In addition, the pore space formed by silt and sand particles with large diameters is not filled by clay particles because there are no (or few) clay particles, so the silty fine sand has larger porosity and wider pore water seepage channels.

(2) The clay particles in the silt are evenly distributed around the silt and sand particles, and the large-diameter silt and sand particles are wrapped, which is similar to the structure of the soil sample (clay content 11%) photographed by Gratchev et al. (2006) using SEM. The clay particles covering the surface of large particles play a role similar to an "adhesive", connecting the large particles on both sides, blocking the seepage channel, and reducing the permeability of soil, which is not possessed by silty fine sand.

Therefore, based on the results of the consolidation permeability experiments and discrete element simulations, the macroscopic and microscopic reasons for the differences in pore pressure response and liquefaction behavior of the two soil beds under wave action can be depicted in Fig. 12.

The deformation abilities of silt and silty fine sand under external forces differ. When cyclic normal and shear stresses induced by wave loading act on the silt bed, it is more prone to generate larger plastic volumetric strains, leading to a densification of the soil bed. From a microscopic perspective, the presence of clay particles in silt results in smaller pore spaces between soil particles and narrower seepage channels, leading to poor soil permeability. Under the external wave load of high amplitude and frequency, the water in the internal pores of silt bed cannot be drained after the silt becomes denser. The pore water is "retention" in the soil skeleton, resulting in the accumulation of pore water pressure. When the accumulated excess pore pressure reaches the initial effective stress of the overburden soil, liquefaction occurs in the silt bed. On the contrary, the plastic volumetric

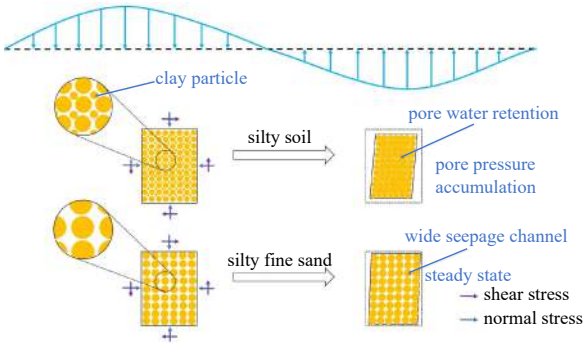

Fig. 12. Schematic diagram of pore water pressure response difference between silt and silty fine sand beds.

strain of silty fine sand bed under wave loading is very small, and the soil skeleton structure can maintain stability. Simultaneously, the silty fine sand is characterized by the absence or minimal presence of clay particles, resulting in larger pore spaces between soil particles and wider seepage channels, ultimately leading to greater permeability. Therefore, the pore water pressure within the soil only exhibits an elastic response to wave loads, without accumulating pore water pressure.

3.3 *Discrete element simulation of consolidation experiments for silt and silty fine sand*

Figure 13 illustrates the evolution of micro arrangement characteristics of particles in silt and silty fine sand during consolidation loading. It can be observed that during the process of consolidation loading, there are significant changes in the arrangement of particles within the silt. In contrast, the silty fine sand exhibits a small compression displacement, therefore, there is no noticeable change in the arrangement of particles during compression. As compression proceeds, particles in the silt undergo significant vertical displacement, causing the originally larger pore spaces to decrease in size due to the intrusion of smaller particles (Fig. 13a). The magnitude of the contact force between particles can be indicated by the amount of particle overlap. The greater the degree of overlap, the stronger the contact force between particles. After consolidation loading, the overlap between internal particles of the silt increases noticeably, indicating a tighter contact between the particles. Additionally, due to the cohesive forces of clay particles, the permeability coefficient of the silt experiences a significant decrease during the compression process. The internal pore space of silty fine sand does not exhibit significant changes before and after consolidation loading (Fig. 13b). As a result, the permeability coefficient experiences only minimal decline following consolidation compression.

Ren et al. (2020a) found through flume experiments and theoretical calculations that the initial failure mode of a silt bed with a high degree of consolidation (consolidated for 7 days, Test 1) under wave loading is shear failure, while the initial failure mode of a silt bed with a low degree of consolidation (consolidated for 4 h, Test 2) is liquefaction (Fig. 14). After the initial failure, the two kinds of soil bed are subject to progressive liquefaction from top to bottom. However, no explanation is given for this phenomenon.

The discrete element simulation of the consolidation experiment on silt may provide a microscopic explanation for this phenomenon. When the degree of consolidation of the silt bed is high, the contact between particles inside the silt is tighter, and the cohesive effect of clay particles causes the highly consolidated silt bed to form a “whole” (Fig.14a). When the shear stress

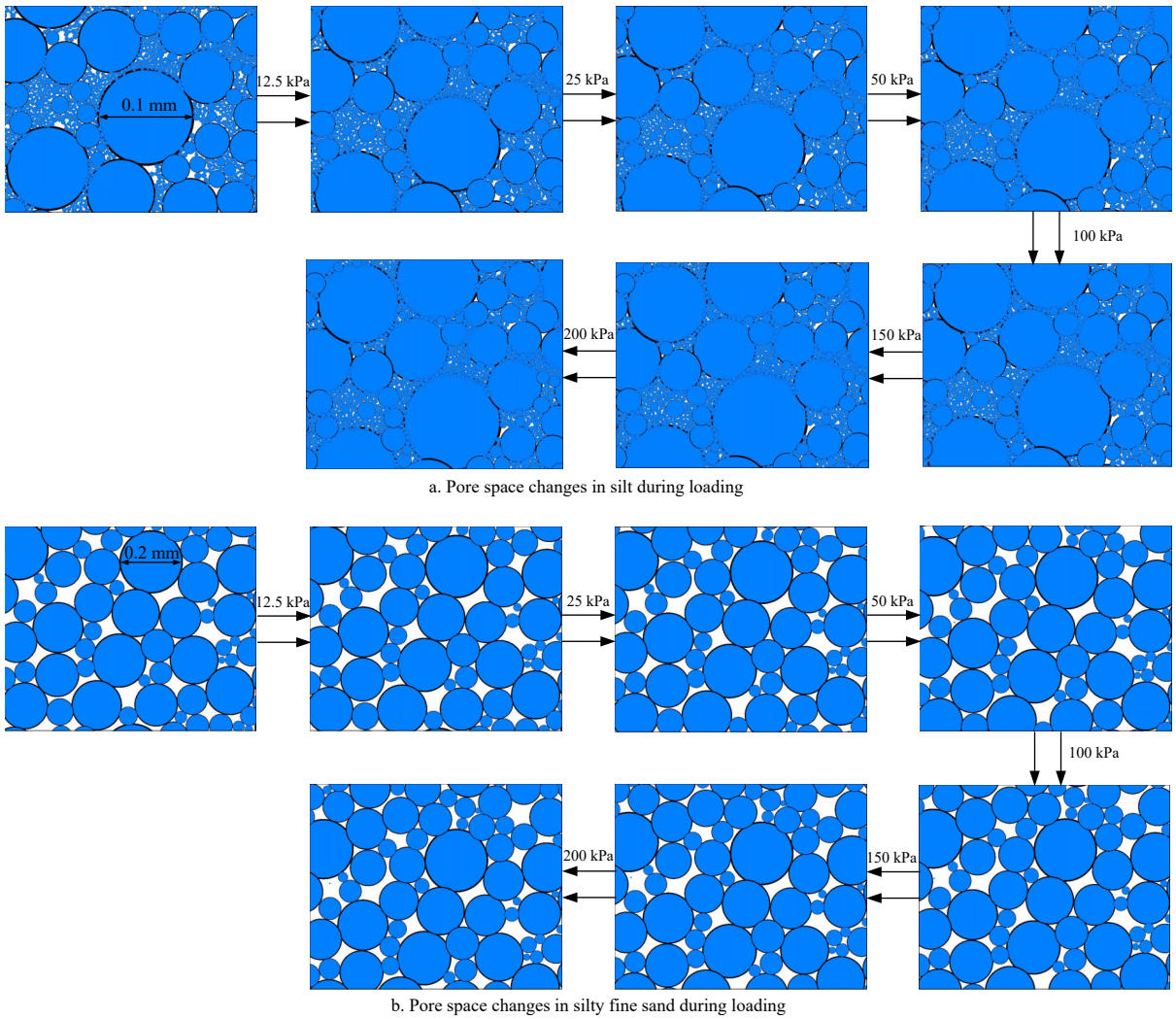

a. Pore space changes in silt during loading

b. Pore space changes in silty fine sand during loading

Fig. 13. The evolution of the soil pore space during loading.

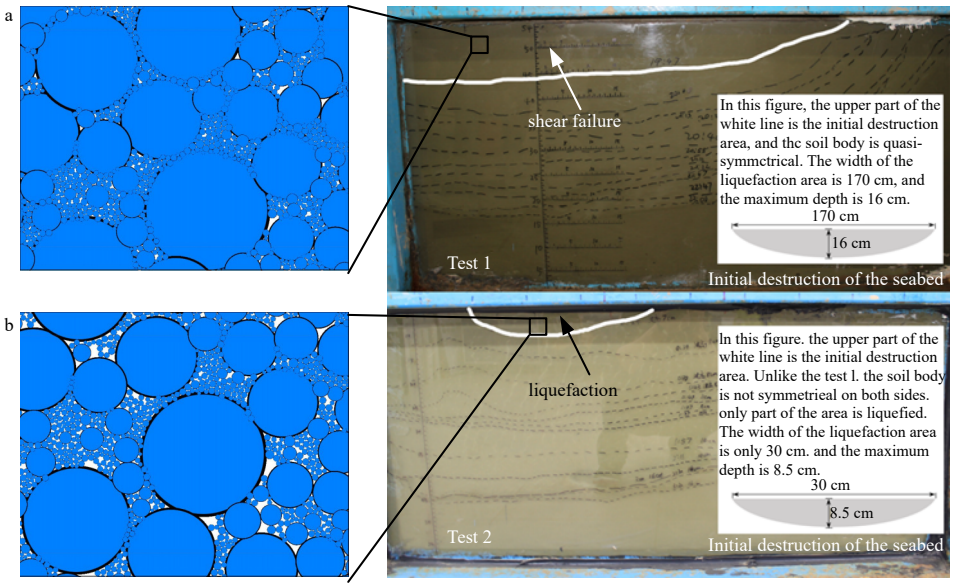

Fig. 14. Initial failure mode of the silt bed under different degrees of consolidation (Ren et al., 2020a).

caused by waves exceeds the shear strength of a weak point in the silt bed, initial shear failure occurs. When the degree of consolidation of the silt bed is low, the particles inside the silt are loosely arranged, and the pore space between particles is larger. The silt still has a relatively open microfabric (Fig.14b). Under the action of wave loads, the connection between soil particles is destroyed, and the internal pore pressure accumulates. Soil particles disperse into the fluid and initial liquefaction failure occurs.

4 Conclusions

In this paper, a flume experiment to investigate the differences in pore water pressure response and liquefaction behavior of silt and silty fine sand beds with different particle compositions under wave action. Furthermore, the reasons for these differences were analyzed from both macroscopic and microscopic perspectives. Additionally, the microscale reasons for the distinct initial failure modes exhibited by soil beds with varying degrees of consolidation were investigated through the discrete element simulations. The conclusions are as following:

(1) The silt bed is more prone to liquefaction than the silty fine sand bed. Specifically, the silt bed requires less wave load intensity to reach the liquefaction state, the liquefaction depth of the silt bed is greater, and the liquefaction duration is longer. The main cause of the differential response in pore water pressure between two soil beds is the difference in permeability and plastic deformation under external forces. Compared to silty fine sand, silt exhibits lower permeability and is more prone to plastic deformation under external forces, thereby causing easier accumulation of pore water pressure and leading to liquefaction.

(2) The micro arrangement characteristics of particles in silt and silty fine sand exhibits distinct characteristics. The pore space and seepage channels of silt are smaller, and the permeability is worse because of clay particles in silt. At the same time, when the degree of consolidation is low, the particles in the silt are loosely arranged, and the soil is still a relatively open microfabric. When the degree of consolidation is high, the particles contact more closely, forming a “whole”, which makes the silt bed have different initial failure modes under different degrees of consolidation.

References

Biot M A. 1956. Theory of propagation of elastic waves in a fluid-saturated porous solid. I. low-frequency range. The Journal of the Acoustical Society of America, 28(2): 168–178, doi: 10.1121/1.1908239

Cao Ruichen, Wang Shuya, Xu Guohui, et al. 2019. Characteristics of liquefied soil motion in wavy environment. Physics of Fluids, 31(7): 073102, doi: 10.1063/1.5098507

Chen Changyun, Xu Guohui, Ren Yupeng, et al. 2019. Measurement of the viscosity coefficient of liquefied silty soil. Geo-Marine Letters, 39(2): 135–148, doi: 10.1007/s00367-019-00563-5

de Groot M B, Kudella M, Meijers P, et al. 2006. Liquefaction phenomena underneath marine gravity structures subjected to wave loads. Journal of Waterway, Port, Coastal, and Ocean Engineering, 132(4): 325–335,doi: 10.1061/(ASCE)0733-950X(2006)132:4(325)

Duan Lunliang, Jeng D S, Wang Shaohua, et al. 2019. Numerical investigation of the wave/current-induced responses of transient soil around a square mono-pile foundation. Journal of Coastal Research, 35(3): 625–636, doi: 10.2112/JCOASTRES-D-18-00072.1

Duan Lunliang, Liao Chencong, Jeng D S, et al. 2017. 2D numerical study of wave and current-induced oscillatory non-cohesive soil liquefaction around a partially buried pipeline in a trench. Ocean Engineering, 135: 39–51, doi: 10.1016/j.oceaneng.2017.02.036

Foda M A, Tzang S Y. 1994. Resonant fluidization of silty soil by water waves. Journal of Geophysical Research:Oceans, 99(C10): 20463–20475, doi: 10.1029/94JC02040

Gao Yufeng, Shen Yang, Zhang Jian, et al. 2011. Analysis of wave-induced liquefaction in seabed deposits of silt. China Ocean Engineering, 25(1): 31–44, doi: 10.1007/s13344-011-0003-z

Gratchev I B, Sassa K, Osipov V I, et al. 2006. The liquefaction of clayey soils under cyclic loading. Engineering Geology, 86(1): 70–84, doi: 10.1016/j.enggeo.2006.04.006

Guo Zhen, Jeng D S, Guo Wei. 2014. Simplified approximation of wave-induced liquefaction in a shallow porous seabed. International Journal of Geomechanics, 14(4): 06014008, doi: 10.1061/(ASCE)GM.1943-5622.0000366

Jeng D S. 1997. Wave-induced seabed instability in front of a breakwater. Ocean Engineering, 24(10): 887–917, doi: 10.1016/S0029-8018(96)00046-7

Jeng D S, Cha D H. 2003. Effects of dynamic soil behavior and wave non-linearity on the wave-induced pore pressure and effective stresses in porous seabed. Ocean Engineering, 30(16):

2065–2089, doi: 10.1016/S0029-8018(03)00070-2
Jeng D S, Rahman M S. 2000. Effective stresses in a porous seabed of finite thickness: inertia effects. Canadian Geotechnical Journal, 37(6): 1383–1392, doi: 10.1139/t00-063
Kirca V S O. 2013. Sinking of irregular shape blocks into marine seabed under wave-induced liquefaction. Coastal Engineering, 75: 40–51, doi: 10.1016/j.coastaleng.2013.01.006
Kirca V S O, Sumer B M. 2018. Sinking failure of drag embedment anchors due to wave-induced seabed liquefaction. International Journal of Ocean and Coastal Engineering, 1(4): 1850006, doi: 10.1142/S2529807018500069
Kirca V S O, Sumer B M, Fredsøe J. 2013. Residual liquefaction of seabed under standing waves. Journal of Waterway, Port, Coastal, and Ocean Engineering, 139(6): 489–501,doi: 10.1061/(ASCE)WW.1943-5460.0000208
Kirca V S O, Sumer B M, Fredsøe J. 2014. Influence of clay content on wave-induced liquefaction. Journal of Waterway, Port, Coastal, and Ocean Engineering, 140(6): 04014024,doi: 10.1061/(ASCE)WW.1943-5460.0000249
Liu Zhuangyi, Jeng D S, Chan A H C, et al. 2009. Wave - induced progressive liquefaction in a poro-elastoplastic seabed: a two - layered model. International Journal for Numerical and Analytical Methods in Geomechanics, 33(5): 591–610, doi: 10.1002/nag.734
Liu Bo, Jeng D S, Ye Guanlin, et al. 2015. Laboratory study for pore pressures in sandy deposit under wave loading. Ocean Engineering, 106: 207–219, doi: 10.1016/j.oceaneng.2015.06.029
Madsen O S. 1978. Wave-induced pore pressures and effective stresses in a porous bed. Géotechnique, 28(4): 377–393, doi: 10.1680/geot.1978.28.4.377
Miyamoto J, Sassa S, Sekiguchi H. 2004. Progressive solidification of a liquefied sand layer during continued wave loading. Géotechnique, 54(10): 617–629, doi: 10.1680/geot.2004.54.10.617
Miyamoto J, Sassa S, Tsurugasaki K, et al. 2020. Wave-induced liquefaction and floatation of a pipeline in a drum centrifuge. Journal of Waterway, Port, Coastal, and Ocean Engineering, 146(2): 04019039,doi: 10.1061/(ASCE)WW.1943-5460.0000547
Okusa S. 1985. Wave-induced stresses in unsaturated submarine sediments. Géotechnique, 35(4): 517–532, doi: 10.1680/geot.1985.35.4.517
Peng Changsheng, Liu Hui, Zhang Qian, et al. 2015. Effects of particle size and solution properties on permeability of porous media. Periodical of Ocean University of China (in Chinese), 45(3): 107–115, doi: 10.16441/j.cnki.hdxb.20130409
Prior D B, Suhayda J N, Lu Nianzu, et al. 1989. Storm wave reactivation of a submarine landslide. Nature, 341(6237): 47–50, doi: 10.1038/341047a0
Ren Yupeng, Xu Guohui, Xu Xingbei, et al. 2020a. The initial wave induced failure of silty seabed: liquefaction or shear failure. Ocean Engineering, 200: 106990, doi: 10.1016/j.oceaneng.2020.106990
Ren Yupeng, Xu Xingbei, Xu Guohui, et al. 2020b. Measurement and calculation of particle trajectory of liquefied soil under wave action. Applied Ocean Research, 101: 102202, doi: 10.1016/j.apor.2020.102202
Ren Yupeng, Zeng Yu, Xu Xingbei, et al. 2021. Sedimentary changes of a sand layer in liquefied silts. Journal of Ocean University of China, 20(5): 1046–1054, doi: 10.1007/s11802-021-4624-4
Sassa S, Sekiguchi H. 1999. Wave-induced liquefaction of beds of sand in a centrifuge. Géotechnique, 49(5): 621–638, doi: 10.1680/geot.1999.49.5.621
Sassa S, Sekiguchi H. 2001. Analysis of wave-induced liquefaction of sand beds. Géotechnique, 51(2): 115–126, doi: 10.1680/geot.2001.51.2.115
Sassa S, Sekiguchi H, Miyamoto J. 2001. Analysis of progressive liquefaction as a moving-boundary problem. Géotechnique, 51(10): 847–857, doi: 10.1680/geot.2001.51.10.847
Sassa S, Takayama T, Mizutani M, et al. 2006. Field observations of the build-up and dissipation of residual pore pressures in seabed sands under the passage of storm waves. Journal of Coastal Research, 39: 410–414
Sumer B M, Dixen F H, Fredsøe J. 2011. Stability of submerged rock berms exposed to motion of liquefied soil in waves. Ocean Engineering, 38(7): 849–859, doi: 10.1016/j.oceaneng.2010.09.009
Sumer B M, Fredsøe J, Christensen S, et al. 1999. Sinking/floatation of pipelines and other objects in liquefied soil under waves. Coastal Engineering, 38(2): 53–90, doi: 10.1016/S0378-3839(99)00024-1
Sumer B M, Hatipoglu F, Fredsøe J, et al. 2006a. Critical flotation density of pipelines in soils liquefied by waves and density of liquefied soils. Journal of Waterway, Port, Coastal, and Ocean Engineering, 132(4): 252–265, doi: 10.1061/(ASCE)0733-950X(2006)132:4(252)
Sumer B M, Hatipoglu F, Fredsøe J, et al. 2006b. The sequence of sediment behaviour during wave-induced liquefaction. Sedimentology, 53(3): 611–629, doi: 10.1111/j.1365-3091.2006.00763.x
Sumer B M, Truelsen C, Fredsøe J. 2006c. Liquefaction around pipelines under waves. Journal of Waterway, Port, Coastal, and Ocean Engineering, 132(4): 266–275, doi: 10.1061/(ASCE)0733-950X(2006)132:4(266)
Tsai C P. 1995. Wave-induced liquefaction potential in a porous seabed in front of a breakwater. Ocean Engineering, 22(1): 1–18, doi: 10.1016/0029-8018(94)00042-5
Tzang S Y, Ou S H. 2006. Laboratory flume studies on monochromatic wave-fine sandy bed interactions: Part 1. Soil fluidization. Coastal Engineering, 53(11): 965–982, doi: 10.1016/j.coastaleng.2006.06.003
Wang Yuchen, Oh E, Zhan Jiemin. 2016. Examining the behaviors of sandy and silty seabed under wave actions. Journal of Marine Science and Technology, 24(4): 682–689, doi: 10.6119/JMST-015-1231-1
Wu Sheng, Jeng D S. 2019. Effects of dynamic soil permeability on the wave-induced seabed response around a buried pipeline. Ocean Engineering, 186: 106132, doi: 10.1016/j.oceaneng.2019.106132
Xu Guohui, Liu Zhiqin, Sun Yongfu, et al. 2016. Experimental characterization of storm liquefaction deposits sequences. Marine Geology, 382: 191–199, doi: 10.1016/j.margeo.2016.10.015
Xu Guohui, Sun Yongfu, Wang Xin, et al. 2009. Wave-induced shallow slides and their features on the subaqueous Huanghe River delta. Canadian Geotechnical Journal, 46(12): 1406–1417, doi: 10.1139/T09-068
Xu Guohui, Sun Yongfu, Yu Yueqian, et al. 2012. Discussion on storm-induced liquefaction of the superficial stratum in the Huanghe River subaqueous delta. Marine Science Bulletin, 14(1): 80–89
Xu Xingbei, Xu Guohui, Ren Yupeng, et al. 2019. Horizontal normal force on buried rigid pipelines in fluctuant liquefied silty soil. Journal of Ocean University of China, 18(1): 1–8, doi: 10.1007/s11802-019-3526-1
Xu Xingbei, Xu Guohui, Yang Junjie, et al. 2021. Field observation of the wave-induced pore pressure response in a silty soil seabed. Geo-Marine Letters, 41(1): 13, doi: 10.1007/s00367-020-00680-6
Yamamoto T, Koning H L, Sellmeijer H, et al. 1978. On the response of a poro-elastic bed to water waves. Journal of Fluid Mechanics, 87(1): 193–206, doi: 10.1017/S0022112078003006
Yang Guoxiang, Ye Jianhong. 2017. Wave & current-induced progressive liquefaction in loosely deposited seabed. Ocean Engineering, 142: 303–314, doi: 10.1016/j.oceaneng.2017.07.027
Yang Guoxiang, Ye Jianhong. 2018. Nonlinear standing wave-induced liquefaction in loosely deposited seabed. Bulletin of Engineering Geology and the Environment, 77(1): 205–223, doi: 10.1007/s10064-017-1038-z
Ye Jianhong. 2012. 3D liquefaction criteria for seabed considering the cohesion and friction of soil. Applied Ocean Research, 37: 111–119, doi: 10.1016/j.apor.2012.04.004
Ye Jianhong, He Kunpeng. 2021. Dynamics of a pipeline buried in loosely deposited seabed to nonlinear wave & current. Ocean Engineering, 232: 109127, doi: 10.1016/j.oceaneng.2021.109127
Ye Jianhong, Jeng D, Wang Ren, et al. 2013. Validation of a 2-D semi-

coupled numerical model for fluid–structure–seabed interaction. Journal of Fluids and Structures, 42: 333–357, doi: 10.1016/j.jfluidstructs.2013.04.008

Ye Guanlin, Leng Jian, Jeng D S. 2018. Numerical testing on wave-induced seabed liquefaction with a poro-elastoplastic model. Soil Dynamics and Earthquake Engineering, 105: 150–159, doi: 10.1016/j.soildyn.2017.11.026

Ye Jianhong, Wang Gang. 2015. Seismic dynamics of offshore breakwater on liquefiable seabed foundation. Soil Dynamics and Earthquake Engineering, 76: 86–99, doi: 10.1016/j.soildyn.2015.02.003

Zen K, Yamazaki H. 1990a. Mechanism of wave-induced liquefaction and densification in seabed. Soils and Foundations, 30(4): 90–104, doi: 10.3208/sandf1972.30.4_90

Zen K, Yamazaki H. 1990b. Oscillatory pore pressure and liquefaction in seabed induced by ocean waves. Soils and Foundations, 30(4): 147–161, doi: 10.3208/sandf1972.30.4_147

Zen K, Yamazaki H. 1991. Field observation and analysis of wave-induced liquefaction in seabed. Soils and Foundations, 31(4): 161–179, doi: 10.3208/sandf1972.31.4_161

Zhang Jun, Jiang Qin, Jeng D, et al. 2020. Experimental study on mechanism of wave-induced liquefaction of sand-clay seabed. Journal of Marine Science and Engineering, 8(2): 66, doi: 10.3390/jmse8020066

Zhao Hongyi, Jeng D S, Liao Chencong. 2016. Parametric study of the wave-induced residual liquefaction around an embedded pipeline. Applied Ocean Research, 55: 163–180, doi: 10.1016/j.apor.2015.12.005

Zhao Hongyi, Jeng D S, Liao Chencong, et al. 2018. Numerical modelling of liquefaction in loose sand deposits subjected to ocean waves. Applied Ocean Research, 73: 27–41, doi: 10.1016/j.apor.2018.01.011

Zienkiewicz O C, Chang C T, Bettess P. 1980. Drained, undrained, consolidating and dynamic behaviour assumptions in soils. Géotechnique, 30(4): 385–395, doi: 10.1680/geot.1980.30.4.385